


Zero-index metamaterials for Dirac fermion in graphene

Yinghui Ren, Pengcheng Wan, Ling Zhou, Ruihuang Zhao, Qianjing Wang, Di Huang, Haiqin Guo, and Junjie Du^{*}
Key Laboratory of Polar Materials and Devices, Ministry of Education, School of Physics and Electronic Science, East China Normal University, Shanghai 200062, China

 (Received 20 October 2020; revised 9 February 2021; accepted 11 February 2021; published 22 February 2021)

We study the response of ballistic electron waves in graphene to a square array composed of gate-defined quantum dots when the incident energy is at the neutral point of the Dirac conical dispersion. The effective medium theory shows that the array will behave as a zero-refractive-index medium. Our simulations based on the rigorous multiple scattering theory corroborate that it can indeed exhibit various typical applications of zero-refractive-index media, such as the focusing effect of electron waves, the control over the propagation direction, and directional emission. The array is usually about one-wavelength thick so that the incident wave can penetrate it and the wave front can be tailored by engineering the geometrical shape of the emergent surface. The wave-manipulating behaviors based on zero-index metamaterials could open unprecedented opportunities to steer the flow of graphene electrons in novel manners and shape the wave front of electron beams at will.

DOI: [10.1103/PhysRevB.103.085431](https://doi.org/10.1103/PhysRevB.103.085431)

I. INTRODUCTION

Since graphene's initial discovery, it has been attracting a great deal of interest for its great potential to take microelectronic technologies to new levels based on its exotic electrical properties, including high carrier mobility, high electrical conductivity, ballistic transport at the micron scale under ambient temperatures, and so on [1]. The exceptional chemical [2], mechanical [3,4], thermal [5], and optical [6] properties endow graphene with opportunities to develop electronic elements with unique performance. As an example, graphene-based transparent conductive coatings [7,8] can be designed as touchscreen displays, foldable organic light-emitting diodes, and rollable electronic paper. Various functional devices such as transistors [9], quantum capacitors [10], electron waveguides [11–13], splitters [14,15], and inductors [16] have been proposed. Various mechanisms of controlling the flow of graphene electrons are used in developing such functional devices, among which is the similarity between low-energy graphene electrons and light waves based on the fact that electrons in graphene have lightlike dispersion. It has inspired the development of quantum electron optics in graphene and great progress has been made to manipulate electron waves in similar ways that are often used in optics. As a result, transistors [17], electron waveguides [18], two-dimensional Dirac fermion microscope [19,20], interferometers [21,22], collimators [23], couplers [24], and so on have been successively designed based on the theory of electron optics.

In recent decades, optical metamaterials have exhibited peculiar optical properties, in contrast to naturally occurring optical materials, since they can possess arbitrary desired electromagnetic susceptibilities [25]. Negative and zero refractive indexes have been obtainable in metamaterials to which

electromagnetic waves will respond in a counterintuitive way [26–31]. Fortunately, negative refraction has been extended to graphene, and Veselago lenses for electron waves have been explored [32–34]. However, zero-refractive-index metamaterials for Dirac fermions in graphene have not been extensively studied so far. Physically, the spatial and temporal field variations will decouple and waves will propagate with infinite wavelength and phase velocity in zero-refractive-index media. The peculiar properties enable it to exhibit a wealth of fascinating applications which have been widely studied in optics such as tunneling waveguides [35], directional emission [36], beam steering [31], electromagnetic cloaks [37,38], and so on.

The analogies between optics and low-energy electronics in monolayer graphene inspires us to explore, in this work, the possibilities of constructing Dirac fermion metamaterials with zero refractive index to control graphene ballistic electrons. In general, the effective refractive index of a potential zone is zero when the incident electron energy is equal to the potential applied to the zone since the refractive index is defined as $n = |E - V|/E$. However, the incident energy actually resides at the Dirac point in the conical dispersion of graphene at this moment. It is a well-known fact that graphene has poor conductivity at the Dirac point, though it is not zero because of the so-called minimum conductivity [39–43]. In addition, graphene near charge neutrality probably behaves as a “Dirac fluid,” instead of a Fermi liquid, and exhibits a quantum-critical relativistic plasma behavior. As a result, zero-refractive-index metamaterials have not been considered as a feasible platform to manipulate graphene electrons. However, as will be shown in our studies, this does not mean that the concept of zero refractive index necessarily fails to apply to graphene. Our studies demonstrate that near-normal-incidence electrons at the Dirac energy can pass through a near-wavelength-thick material with near-unity efficiency. This is because the incident wave will enter the zero-index material in the form of evanescent waves when encountering

^{*}phyjunjie@gmail.com

it, instead of being reflected immediately. The evanescent modes help the wave penetrate the material that is thinner than wavelength with nearly 100% efficiency. Moreover, the electrons which travel out from the materials will behave in accordance with the properties of zero-refractive-index media, allowing one to impose a control over the electrons. Finally, it should be noted that the Dirac point energy does not imply that the electrons in our systems necessarily behave as a Dirac fluid. The description of a Fermi liquid holds true in appropriate temperatures and the carrier densities, as shown in Ref. [44].

In this paper, we will construct a square-lattice array of quantum dots (QDs) to realize zero-refractive-index Dirac fermion metamaterials. In previous research, an effective medium theory was developed to calculate the effective refractive index of Dirac fermion metamaterials consisting of QDs [45]. This allows us to theoretically design a metamaterial with an arbitrary refractive index using QDs with a controllable bias. Very recently, nanoscale QDs with atomically sharp boundaries have been obtainable in experiment [46–48]. The fabrication techniques of high-precision QDs [46–49] make it possible to realize such metamaterials. In Sec. II, we will give a brief description of the retrieval of the zero refractive index and identify a zero-refractive-index material for which an effective medium theory can be satisfactorily applied. In Sec. III, we will demonstrate various behaviors of electron waves when they strike the designer zero-refractive-index material. Three characteristic phenomena in zero-refractive-index media will be presented, including wave-front modulation, beam steering, and directional emission.

II. THEORETICAL DESIGN OF ZERO-INDEX METAMATERIALS

An analytic formulation of an effective “refractive index” has been derived based on the coherent-potential approximation for low-energy graphene electron waves in an array of QDs [45]. It is applicable when the scattering of electrons by a circular QD can be described by the single-valley Hamiltonian [50–56]

$$H = -i\nabla\sigma + V_s\Theta(r_s - r), \quad (1)$$

where $\sigma = (\sigma_x, \sigma_y)$ are Pauli matrices, V_s is the potential applied to the QD, $\Theta(r_s - r)$ is the Heaviside step function, and r_s is the radius of the QD. The description for the behaviors of electrons in Eq. (1) holds when the Fermi wavelength λ_F of Dirac electrons is much larger than the gradual transition ΔR of potentials in the boundary of the circular QD (i.e., $\lambda_F \gg \Delta R$). Meanwhile, ΔR should be smaller than $0.5r_s$ [57] so that the electron scattering behaviors of the QDs are not affected by the grading width, but are much larger than the graphene’s intrinsic lattice constant to forbid the umklapp scattering between different valleys in the graphene. The reduced units are employed throughout with $\hbar = 1$ and the Fermi velocity $v_F = 1$, unless noted otherwise.

The electron waves obeying the Hamiltonian in Eq. (1) will have a linear lightlike dispersion relation in the low-energy region, allowing the extension of the effective media theory for light to graphene electronics. Thus, a periodic QD array

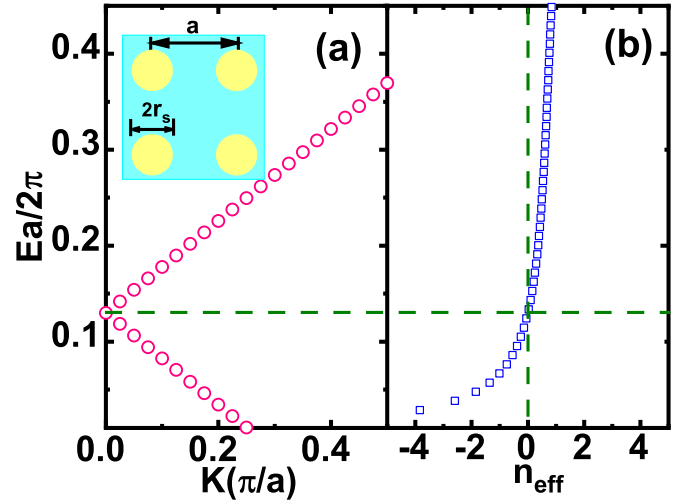


FIG. 1. (a) The energy band structures of the square array of the QDs with the radius of the QDs $r_s = 1.0$, the lattice constant $a = 4.0$, and the potential applied on the QDs, $V_s = 1.0$. They are calculated using the rigorous multiple scattering theory. (b) The effective “refractive index” n_{eff} vs $\tilde{E} = Ea/2\pi$, obtained from the coherent-potential approximation. The inset in (a) indicates the geometric configuration of the square-lattice array.

can be handled as a uniform medium when both the dimension of the QDs and the lattice spacing are smaller than the electron wavelength. The QDs behave as an artificial atom/molecule with respect to the wavelength. The effective “refractive index” of a two-dimensional array is given by Ref. [45],

$$n_{eff} = \frac{2[J_1(k_o r_o) + D_0(o)H_1^{(1)}(k_o r_o)]}{k_o r_o [J_0(k_o r_o) + D_{-1}(o)H_0^{(1)}(k_o r_o)]}, \quad (2)$$

where

$$D_m(o) = \frac{-J_m(k_o r_s)J_{m+1}(k_s r_s) + \alpha\alpha' J_{m+1}(k_o r_s)J_m(k_s r_s)}{J_{m+1}(k_s r_s)H_m^{(1)}(k_o r_s) - \alpha\alpha' J_m(k_s r_s)H_{m+1}^{(1)}(k_o r_s)} \quad (3)$$

are the Mie scattering coefficients of the QDs [49,50,55,56]. For the square-lattice array depicted schematically in the inset of Fig. 1(a), $r_o = \frac{a}{\sqrt{\pi}}$ represents the radius of the coated potential, with a the lattice constant. The coated potential in the coherent-potential approximation is an equal-area region of the unit cell of the system, with the QD as the inner core and the background medium as the coated layer. The effective refractive index n_{eff} is determined by the condition that the total scattering of a coated potential in the effective medium vanishes in the limit $k_e r_o \ll 1$, where $k_e = n_{eff} k_o$, with k_o and k_e the wave number in the background medium and the effective medium, respectively. J_m and $H_m^{(1)}$ are, respectively, the m th-order Bessel function and Hankel function of the first kind, and k_s is the wave number in the QD region. The “band indices” α and α' are defined as $\alpha = \text{sgn}(E)$ and $\alpha' = \text{sgn}(E - V_s)$, with E the energy of the incident electrons. The QDs embedded in a background medium with refractive index $n_b = (E - V_b)/E$ are handled as a circular potential, with refractive index $n_s = (E - V_s)/E$. The circular potential can be considered infinitely high in size in contrast to one-atom-thick graphene, and thus a two-dimensional model is applicable to the problem. V_b is the potential applied in the background and

is set to 0 without loss of generality (i.e., the refractive index of the background, $n_b = 1$).

The energy band structures of the system with $a = 4$, $r_s = 1$, and $V_s = 1$ are calculated using the rigorous multiple scattering theory [24,45] and are shown in Fig. 1(a). One can see that a Dirac cone dispersion exists about the Γ point ($k = 0$). We use Eq. (2) to calculate its effective refractive index, which is given as a function of the incident energy in Fig. 1(b). We see that n_{eff} goes from negative to positive with the energy increasing. The comparison between Figs. 1(a) and 1(b) shows that the slope of the bands is consistent with the sign of n_{eff} near $k = 0$. Above the Dirac point, the band has a positive slope and corresponds to positive refractive indices, while a negative slope below the Dirac point is related to negative refractive indices. As a result, the near-zero refractive indices appear near the Dirac point energy. There is actually one correspondence between a Dirac point and a zero refractive index, as has been revealed in nano-optics [37]. However, a Dirac cone dispersion does not always imply a zero refractive index. To achieve a zero refractive index, the Dirac cone is required to be at $k = 0$. In the following, we will use the square array to simulate a zero-refractive-index medium in graphene and perform a proof-of-principle demonstration for its wave-manipulating behavior. We also explore the possibilities to construct a zero-index metamaterial based on quantum antidots [58,59] since they can be prepared through current experimental techniques, but unfortunately our calculation shows the approach is not feasible. In this paper, the QD radius $r_s = 1$ implies that the quantities with the dimension of length, including the lattice spacing and wavelength, are in units of r_s . Once r_s is known in real units, the lattice spacing is $a = 4r_s$, the wavelength is $\lambda = 2\pi r_s/E$, and thus the incident energy in real units is $E\hbar v_F/r_s$ according to the de Broglie relationship. Accordingly, the bias in real units is $V\hbar v_F/r_s$.

III. RESULTS AND DISCUSSIONS

A. Phenomena in metamaterials with refractive index near zero

One of the appealing extraordinary abilities of zero-refractive-index media is to mold the wave front of the electron beams into shapes that can be designed at will. This arises from the fact that the waves emerging from zero-refractive-index media will propagate along the normal direction of the interface. A simple understanding can be gained from the Snell's law,

$$n_{eff} \sin \theta_i = n_b \sin \theta_t, \quad (4)$$

where n_{eff} is 0 in a zero-refractive-index medium and thus θ_t has to equal 0. In other words, the emergent direction is normal to the interface. The property allows one to control the wave front of the electron waves by tailoring the geometry of the emergent surface of zero-refractive-index media. Naturally, the focusing effect can be expected for the wave coming out of the semicircle-shaped emergent surface because its normal direction is the radial direction and the emergent wave will converge at the center of the semicircle.

To this end, we design a zero-index metamaterial lens which has a semicircle-shaped emergent surface and a planar incident surface in Fig. 2. The zero-index metamaterial is the square QD array studied in Fig. 1. The incident-electron

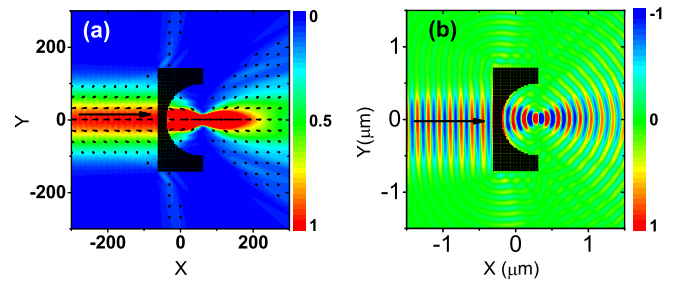


FIG. 2. (a) The electron density and the quiver of local current-density vector around a lens made of the zero-refractive-index metamaterial given in Fig. 1 when illuminated by a Gaussian beam with the Dirac energy $\tilde{E} = Ea/2\pi = 0.13$. (b) The real part of the first spinor component $\text{Re}\{\psi^A\}$ distribution pattern when the lens in (a) is constructed by the QDs in real units. The QD radius is 5 nm and the lattice spacing, incident energy, and bias are 20 nm, 26.8 meV, and 131.6 meV, respectively. The black dots in both panels denote the QDs constituting the lens, which has a planar incident surface and a half-circular concave emergent surface.

energy is set at $\tilde{E} = Ea/2\pi = 0.13$ so that the metamaterial operates at the Dirac point in Fig. 1(a), which implies an effective refractive index $n_{eff} = 0$. Figure 2(a) displays the electron density distribution and the local current-density vector around the zero-index lens when an incident wave strikes the planar surface on the left. One can see that the emergent wave is focused at the center of the semicircle. Here and throughout the paper, all the simulations are carried out based on the Mie scattering theory and the multiple scattering theory. The Mie scattering theory rigorously calculates the electron scattering of a single QD, while the multiple scattering theory handles the scattering problem of a multiple QD system in the case of considering the interaction between all QDs, not the nearest neighbor and the next-nearest neighbor alone.

The focusing can also be understood from the infinite wavelength feature in zero-refractive-index materials. It implies that the propagation distance in it will not cause any phase accumulation, however long or short. For the lens in Fig. 2(a), the difference in propagation distance because of the curved surface does not produce any impact on the phase of the electrons. According to Fermat's principle, an optical system for focusing necessarily satisfies the principle of equal optical path. At the focusing spot, all the electrons have the same phase and therefore the focusing effect is achieved. The zero-index lens is different from Veselago lenses based on negative refraction, where the focal imaging is obtained for a point source. Figure 2 displays a focusing for a parallel electron beam and thus the array can serve as a coupler to couple wide electron beams into various electronic units. To acquire the information about transport when considering the role of couplers, the local current-density vectors are provided in Fig. 2(a) at the same time since the high-resolution imaging of the current flow in monolayer graphene has been achievable in a recent experiment [60].

With the development of the fabrication techniques of high-precision QDs and QD arrays [46–48], it is possible to demonstrate the zero-index behaviors of electrons in

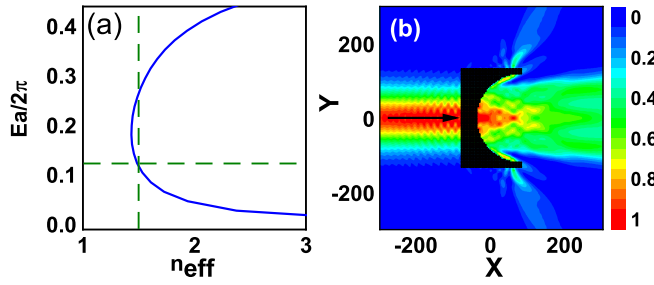


FIG. 3. (a) The effective refractive index n_{eff} vs \tilde{E} for the same square array of the QDs as in Fig. 2, but the potential applied on the QDs is $V_s = -0.4$. The array has the effective refractive index $n_{eff} = 1.5$ at $\tilde{E} = 0.13$. (b) The electron density distribution pattern around the metamaterial with $n_{eff} = 1.5$ when illuminated by a Gaussian beam with the energy $\tilde{E} = Ea/2\pi = 0.13$. The black dots in both panels denote the QDs constituting the metamaterial.

experiment. Typically, the metamaterial in Fig. 2(a) can be composed of the QDs of radius $r_s = 5$ nm. Thus the lattice spacing, incident energy, and the bias are 20 nm, 26.8 meV, and 131.6 meV, respectively. Figure 2(b) shows the real part of the first spinor component, $\text{Re}\psi^A$, around the zero-index lens consisting of such QDs in real units. The thinnest and thickest parts of the lens are about 100 and 600 nm, respectively. Therefore, the focusing process can be completely demonstrated in the total propagation distance of 1 μm . Such a distance is below the mean free path of electrons which is 5.5 μm at 50 K and 2.5 μm at 100 K [61–63] by using appropriate substrates [64]. On the other hand, the electron-electron interaction [65] and the self-consistent interactions of electrons [66] indeed exist within a beam. It means that the focusing effect should be observed at an appropriate temperature and the low carrier densities [62,63], as discussed in the next section.

To exclude the possibility that the focusing effect in Fig. 2 originates from the curved geometries in the lenses, we examine the spatial probability distribution of electrons when the incident energy, the radius of the QDs, and the geometric configuration of the array remain the same, but the potential V_s applied to the QDs is changed. The variation of V_s causes the change of effective refractive index of the metamaterial and the focusing associated with the zero refractive index will disappear. Figure 3(a) displays the effective refractive index n_{eff} when $V_s = -0.4$. We see $n_{eff} = 1.5$ at $\tilde{E} = 0.13$ and the spatial probability distribution in Fig. 3(b) shows that the focusing effect of electrons does not occur though the incident energy and that the geometric features of the array are the same as in Fig. 2. Therefore, it is the zero refractive index rather than the curved geometries in the lenses that leads to the equal optical path and thus the focusing in Fig. 2(b).

Metamaterials have the advantage of robustness in producing functional devices. This can be due to the fact that metamaterials may be regarded as a uniform medium at the operation energy, as indicated by the isotropic band structures around the Γ point in Fig. 1. The slight change of the lattice structure or the radius hardly affects the performance of zero-refractive-index media. To this end, the position disorder and the radius disorder are, respectively, introduced into the metamaterial in Figs. 4(a) and 4(b), with the other parameters

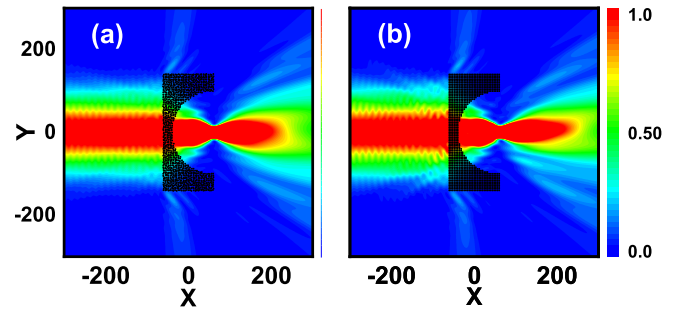


FIG. 4. The electron density distribution around the same zero-index lens as in Fig. 2, with (a) the disorder of position and (b) radius of the QDs introduced.

the same as Fig. 2. The displacement of each QD from its original position is expressed as $d_i = \xi \chi_1 d_{i0}$, with $i = x$ or y , and the variation of the radius is set to be $\Delta r = \zeta \chi_2 d_{i0}$, where ξ and ζ are the random numbers uniformly distributed between -0.5 and 0.5 , χ_1 and χ_2 are the quantities measuring the degree of disorder, and $d_{i0} = a - 2r_s$ is the maximum variation of the radius or position within a unit cell for a square lattice. Here, $\chi_1 = 1$ is chosen, which implies that the QDs can even touch each other, while $\chi_2 = 0.25$ implies that the maximum radius variation is as large as one-fourth of the radius in this structure. The electron density distribution is given in Figs. 4(a) and 4(b), respectively, and show an excellent focusing effect, which bears a close resemblance to that without any disorder in Fig. 2. This illustrates the characteristic nature of metamaterials in which the constituting particles (QDs) behave as artificial molecules or atoms that are much smaller than wavelength. The electron wave cannot sensitively discern the variation of position or radius of the QDs and thus the focusing is not affected.

Our calculations show that electron waves with angle of incidence below 10° can pass through the wavelength-thick array of the QDs with high efficiency. Thus one can expect that the same focusing effect can be observed when an oblique-incidence electron wave encounters the array used in Fig. 2. In Fig. 5(a), we show the electron distribution probability when the incident angle is changed into

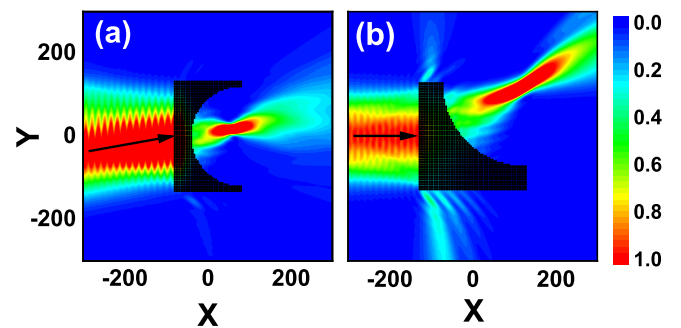


FIG. 5. (a) The electron density distribution around the same lens as in Fig. 2 when the incident angle is $\phi_{inc} = 10^\circ$. (b) The electron density distribution around the lens with a quarter-circular concave emergent surface. In all the cases, the Gaussian beams have the Dirac energy $\tilde{E} = 0.13$ and the arrays have the zero effective refractive index.

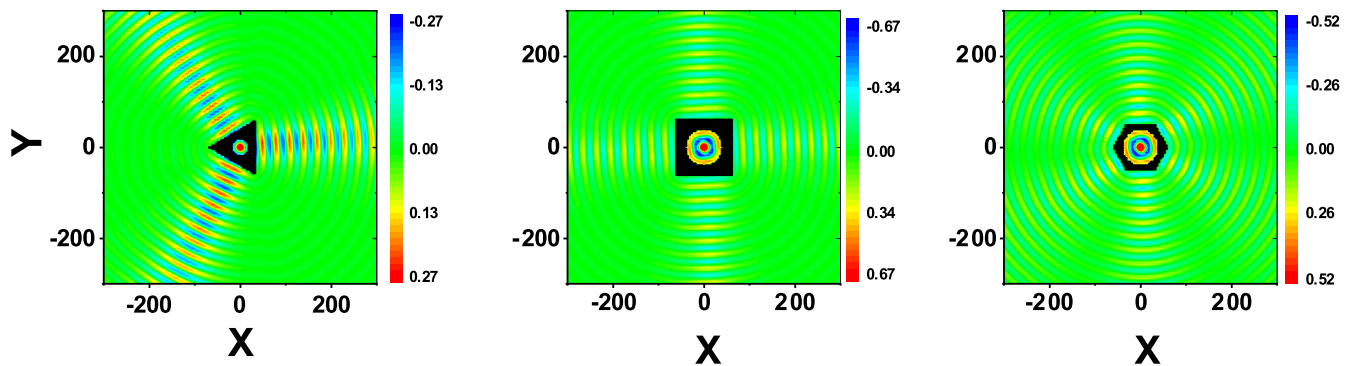


FIG. 6. The real part of the first spinor component, $\text{Re}\{\psi^A\}$, for a (a) three-port, (b) four-port, and (c) six-port emitter. The point sources are placed at the coordinate origin and directional emission can be observed in all of the cases.

$\phi_{inc} = 10^\circ$. As expected, the electron wave is focused on the transmission side again. It shows that the focusing effect is robust to incident angles. This allows us to design a coupler with a certain angle tolerance, which is useful in graphene-based microelectronics. On the other hand, when significantly deviating from the normal incidence, the incident wave hardly enters the zero-refractive-index material. Consequently, the majority of the wave will be reflected and no obvious focusing effect can be observed with the transmittance decaying quickly.

In addition to the control over the wave front, the zero-refractive-index materials can also control the propagation direction of the emergent waves by engineering the orientation of the emergent surfaces. In Fig. 5(b), we design a zero-refractive-index material which has a quarter-circular concave surface on the right side. When a beam of wave normally strikes the left planar surface, the emergent wave is deflected about 45 degrees since it propagates along the radial direction, and is simultaneously focused at the center of the circular concave surface.

Zero-refractive-index metamaterials have been explored to make directional emitters in optics [36,67]. The metamaterials are usually designed as a polyhedron and a point source is placed in its center. Each surface of the polyhedron acts as an emergent port. The waves emerging from the surfaces of the polyhedron propagate along the normal direction of the surfaces. The direction of emission can be controlled by adjusting the orientation of the surfaces and the number of emission is determined by the number of surfaces. In Figs. 6(a)–6(c), respectively, we demonstrate a three-port, four-port, and six-port emitter for graphene electron waves with a point source placed in their centers. All of the ports are comprised of the square QD array studied in Fig. 1. Accordingly, the electrons from the point sources have energy $\tilde{E} = 0.13$ so that the refractive index is zero. The ports are designed to be thinner than wavelength to guarantee that the electrons from the point sources can penetrate through them. The emitters do not need to be excited in a special way, except to place the point source in their center. The propagating wave directionally emits along the predetermined directions out of the emitters no matter how many ports are designed. It shows that the zero-refractive-index materials provide a platform to design directional emitters with flexible emission beam number and arbitrary output boundary.

B. Conditions for experimental observation

In the previous section, we theoretically demonstrated various phenomena which can be achieved in zero-index metamaterials. To make sure that they can be implemented in experiment, the carrier concentration should be $\rho = 10^{11} \text{ cm}^{-2}$ so that beam instability does not occur [66] and the collimated beam propagates as a Fermi fluid [44]. At the same time, the mean free path l is set to be $2 \mu\text{m}$, which is a long enough distance to observe the results, implying a transport relaxation time $\tau = l/v_F = 2 \text{ ps}$. The calculation [61] shows that the carrier mobility is $\mu = 500\,000 \text{ cm}^2/\text{Vs}$ according to $l = h/2e\mu\sqrt{\rho/\pi}$ by taking $\rho = 10^{11} \text{ cm}^{-2}$ and $l = 2 \mu\text{m}$. Such carrier mobility is obtainable under 100 K [62] with an appropriate substrate utilized to eliminate the extrinsic scattering in graphene [61,64].

IV. CONCLUSION

In conclusion, we design a zero-refractive-index Dirac fermion metamaterial by retrieving the effective refractive index of a quantum-dot array with the developed effective media theory for electron waves in graphene. The near-zero refractive index appears near the Dirac point of the conical dispersion of the array. The incident electron beam can penetrate the array when it is one-wavelength thick, though it behaves as a neutral zone. The behavior of the emergent wave is constrained by the zero refractive index of the material and its wave front is always parallel to the emergent surface. Thus the zero-refractive-index material allows for the wave-front shaping and beam steering by engineering the geometry of the emergent surfaces. In addition, the direction emission can also be achieved in a multiple-port emitter when a point source is placed in its center. The artificially structured materials could find applications in designing graphene electron units.

ACKNOWLEDGMENT

We would like to thank Professor Lei Zhang from Shanxi University for helpful discussions. This work was supported by NSFC (Grant No. 11474098).

- [1] A. K. Geim and K. S. Novoselov, *Nat. Mater.* **6**, 183 (2007).
- [2] K. P. Loh, Q. L. Bao, P. K. Ang, and J. X. Yang, *J. Mater. Chem.* **20**, 2277 (2010).
- [3] C. Lee, X. D. Wei, J. W. Kysar, and J. Hone, *Science* **321**, 385 (2008).
- [4] F. Liu, P. B. Ming, and J. Li, *Phys. Rev. B* **76**, 064120 (2007).
- [5] A. A. Balandin, *Nat. Mater.* **10**, 569 (2011).
- [6] R. R. Nair, P. Blake, A. N. Grigorenko, K. S. Novoselov, T. J. Booth, T. Stauber, N. M. R. Peres, and A. K. Geim, *Science* **320**, 1308 (2008).
- [7] S. Bae, H. Kim, Y. Lee, X. F. Xu, J. S. Park, Y. Zheng, J. Balakrishnan, T. Lei, H. R. Kim, Y. I. Song, Y. J. Kim, K. S. Kim, B. Özyilmaz, J.-H. Ahn, B. H. Hong, and S. Iijima, *Nat. Nanotech.* **5**, 574 (2010).
- [8] T. H. Han, Y. Lee, M. R. Choi, S. H. Woo, S. H. Bae, B. H. Hong, J. H. Ahn, and T. W. Lee, *Nat. Photon.* **6**, 105 (2012).
- [9] F. Schwierz, *Nat. Nanotech.* **5**, 87 (2010).
- [10] T. Fang, A. Konar, H. Xing, and D. Jena, *Appl. Phys. Lett.* **91**, 092109 (2007).
- [11] P. Rickhaus, M.-H. Liu, P. Makk, R. Maurand, S. Hess, S. Zihlmann, M. Weiss, K. Richter, and C. Schönenberger, *Nano Lett.* **15**, 5819 (2015).
- [12] M. Kim, J. H. Choi, S. H. Lee, K. Watanabe, T. Taniguchi, S. H. Jhi, and H.-J. Lee, *Nat. Phys.* **12**, 1022 (2016).
- [13] A. Cheng, T. Taniguchi, K. Watanabe, P. Kim, and J. D. Pillet, *Phys. Rev. Lett.* **123**, 216804 (2019).
- [14] P. Brandimarte, M. Engelund, N. Papior, A. Garcia-Lekue, T. Frederiksen, and D. Sánchez-Portal, *J. Chem. Phys.* **146**, 199902 (2017).
- [15] J. Li, R. Zhang, Z. Yin, J. Zhang, K. Watanabe, T. Taniguchi, C. Liu, and J. Zhu, *Science* **362**, 1149 (2018).
- [16] Y. M. Lin, A. Valdes-Garcia, S. J. Han, D. B. Farmer, I. Meric, Y. Sun, Y. Wu, C. Dimitrakopoulos, A. Grill, P. Avouris, and K. A. Jenkins, *Science* **332**, 1294 (2011).
- [17] K. Wang, M. M. Elahi, L. Wang, K. M. M. Habib, T. Taniguchi, K. Watanabe, J. Hone, A. W. Ghosh, G. H. Lee, and P. Kim, *Proc. Natl. Acad. Sci. USA* **116**, 6575 (2019).
- [18] J. R. Williams, T. Low, M. S. Lundstrom, and C. M. Marcus, *Nat. Nanotech.* **6**, 222 (2011).
- [19] A. W. Barnard, A. Hughes, A. L. Sharpe, K. Watanabe, T. Taniguchi, and D. Goldhaber-Gordon, *Nat. Commun.* **8**, 15418 (2017).
- [20] P. Bøggild, J. M. Caridad, C. Stampfer, G. Calogero, N. R. Papior, and M. Brandbyge, *Nat. Commun.* **8**, 15783 (2017).
- [21] A. V. Shytov, M. S. Rudner, and L. S. Levitov, *Phys. Rev. Lett.* **101**, 156804 (2008).
- [22] A. F. Young and P. Kim, *Nat. Phys.* **5**, 222 (2009).
- [23] C. H. Park, Y. W. Son, L. Yang, M. L. Cohen, and S. G. Louie, *Nano Lett.* **8**, 2920 (2008).
- [24] Y. Tang, X. Y. Cao, R. Guo, Y. Y. Zhang, Z. Y. Che, F. T. Yannick, W. P. Zhang, and J. J. Du, *Sci. Rep.* **6**, 33522 (2016).
- [25] D. R. Smith, J. B. Pendry, and M. C. K. Wiltshire, *Science* **305**, 788 (2004).
- [26] D. R. Smith, W. J. Padilla, D. C. Vier, S. C. Nemat-Nasser, and S. Schultz, *Phys. Rev. Lett.* **84**, 4184 (2000).
- [27] J. B. Pendry, *Phys. Rev. Lett.* **85**, 3966 (2000).
- [28] U. Leonhardt, *Science* **312**, 1777 (2006).
- [29] J. B. Pendry, D. Schurig, and D. R. Smith, *Science* **312**, 1781 (2006).
- [30] I. Liberal, and N. Engheta, *Nat. Photon.* **11**, 149 (2017).
- [31] V. C. Nguyen, L. Chen, and K. Halterman, *Phys. Rev. Lett.* **105**, 233908 (2010).
- [32] V. V. Cheianov, V. Fal'ko, and B. L. Altshuler, *Science* **315**, 1252 (2007).
- [33] S. Chen, Z. Han, M. M. Elahi, K. M. M. Habib, L. Wang, B. Wen, Y. Gao, T. Taniguchi, K. Watanabe, J. Hone, A. W. Ghosh, and C. R. Dean, *Science* **353**, 1522 (2016).
- [34] B. Brun, N. Moreau, S. Somanchi, V. H. Nguyen, K. Watanabe, T. Taniguchi, J. C. Charlier, C. Stampfer, and B. Hackens, *Phys. Rev. B* **100**, 041401(R) (2019).
- [35] B. Edwards, A. Alu, M. E. Young, M. Silveirinha, and N. Engheta, *Phys. Rev. Lett.* **100**, 033903 (2008).
- [36] S. Enoch, G. Tayeb, P. Sabouroux, N. Guerin, and P. Vincent, *Phys. Rev. Lett.* **89**, 213902 (2002).
- [37] X. Q. Huang, Y. Lai, Z. H. Hang, H. H. Zheng, and C. T. Chan, *Nat. Mater.* **10**, 582 (2011).
- [38] J. Hao, W. Yan, and M. Qiu, *Appl. Phys. Lett.* **96**, 101109 (2010).
- [39] J. Nilsson, A. H. Castro Neto, F. Guinea, and N. M. R. Peres, *Phys. Rev. Lett.* **97**, 266801 (2006).
- [40] J. Tworzydło, B. Trauzettel, M. Titov, A. Rycerz, and C. W. J. Beenakker, *Phys. Rev. Lett.* **96**, 246802 (2006).
- [41] E. V. Gorbar, V. P. Gusynin, V. A. Miransky, and I. A. Shovkovy, *Phys. Rev. B* **66**, 045108 (2002).
- [42] J. H. Chen, C. Jang, S. Adam, M. S. Fuhrer, E. D. Williams, and M. Ishigami, *Nat. Phys.* **4**, 377 (2008).
- [43] Y. W. Tan, Y. Zhang, K. Bolotin, Y. Zhao, S. Adam, E. H. Hwang, S. Das Sarma, H. L. Stormer, and P. Kim, *Phys. Rev. Lett.* **99**, 246803 (2007).
- [44] J. Crossno, J. K. Shi, K. Wang, X. Liu, A. Harzheim, A. Lucas, S. Sachdev, P. Kim, T. Taniguchi, K. Watanabe, T. A. Ohki, and K. C. Fong, *Science* **351**, 1058 (2016).
- [45] Y. H. Ren, Y. C. Gao, P. C. Wan, Q. J. Wang, D. Huang, and J. J. Du, *Phys. Rev. B* **100**, 045422 (2019).
- [46] K. K. Bai, J. J. Zhou, Y. C. Wei, J. B. Qiao, Y. W. Liu, H. W. Liu, H. Jiang, and L. He, *Phys. Rev. B* **97**, 045413 (2018).
- [47] C. Gutierrez, L. Brown, C.-J. Kim, J. Park, and A. N. Pasupathy, *Nat. Phys.* **12**, 1069 (2016).
- [48] K. K. Bai, J. B. Qiao, H. Jiang, H. Liu, and L. He, *Phys. Rev. B* **95**, 201406(R) (2017).
- [49] J. Caridad, S. Connaughton, C. Ott, H. B. Weber, and V. Krstic, *Nat. Commun.* **7**, 12894 (2016).
- [50] R. L. Heinisch, F. X. Bronold, and H. Fehske, *Phys. Rev. B* **87**, 155409 (2013).
- [51] M. I. Katsnelson, F. Guinea, and A. K. Geim, *Phys. Rev. B* **79**, 195426 (2009).
- [52] P. M. Ostrovsky, I. V. Gornyi, and A. D. Mirlin, *Phys. Rev. B* **74**, 235443 (2006).
- [53] M. Hentschel and F. Guinea, *Phys. Rev. B* **76**, 115407 (2007).
- [54] D. S. Novikov, *Phys. Rev. B* **76**, 245435 (2007).
- [55] C. Schulz, R. L. Heinisch, and H. Fehske, *Phys. Rev. B* **91**, 045130 (2015).
- [56] J. Cserti, A. Pályi, and C. Péterfalvi, *Phys. Rev. Lett.* **99**, 246801 (2007).
- [57] A. Pieper, R. L. Heinisch, and H. Fehske, *Europhys. Lett.* **104**, 47010 (2013).
- [58] I. V. Zagorodnev, Zh. A. Devizorova, and V. V. Enaldiev, *Phys. Rev. B* **92**, 195413 (2015).

- [59] Yu. I. Latysheva, A. P. Orlov, A. V. Frolov, V. A. Volkov, I. V. Zagorodnev, V. A. Skuratov, Yu. V. Petrov, O. F. Vyvenko, D. Yu. Ivanov, M. Konczykowski, and P. Monceau, *JETP Lett.* **98**, 214 (2013).
- [60] J.-P. Tetienne, N. Dontschuk, D. A. Broadway, A. Stacey, D. A. Simpson, and L. C. L. Hollenberg, *Sci. Adv.* **3**, e1602429 (2017).
- [61] A. S. Mayorov, R. V. Gorbachev, S. V. Morozov, L. Britnell, R. Jalil, L. A. Ponomarenko, P. Blake, K. S. Novoselov, K. Watanabe, T. Taniguchi, and A. K. Geim, *Nano Lett.* **11**, 2396 (2011).
- [62] M. Lee, J. R. Wallbank, P. Gallagher, K. Watanabe, T. Taniguchi, V. I. Fal'ko, and D. Goldhaber-Gordon, *Science* **353**, 1526 (2016).
- [63] G. H. Lee, G. H. Park, and H. J. Lee, *Nat. Phys.* **11**, 925 (2015).
- [64] S. Adam, E. H. Hwang, V. M. Galitski, and S. Das Sarma, *Proc. Natl. Acad. Sci. USA* **104**, 18392 (2007).
- [65] Q. Li, and S. Das Sarma, *Phys. Rev. B* **87**, 085406 (2013).
- [66] D. Svintsov, *Phys. Rev. B* **101**, 235440 (2020).
- [67] X. T. He, Y. N. Zhong, Y. Zhou, Z. C. Zhong, and J. W. Dong, *Sci. Rep.* **5**, 13085 (2015).